Smart Bionic Morphing Leg Mannequin for Pressure Assessment of Compression Garment

*Bao Yang[1, #], Xi Wang[2, #], Ying Xiong[1], Su Liu[1], Shi-rui Liu[1], Xia Guo[3] and Xiao-ming Tao[1, *]*

[1] Research Centre of Smart Wearable Technology

Nanotechnology Center of Functional and Intelligent Textiles and Apparel

Institute of Textiles and Clothing

The Hong Kong Polytechnic University, Hong Kong, China

[2] Engineering Research Center of Digitized Textile & Apparel Technology

Chinese Ministry of Education

College of Information Science and Technology

Donghua University, Shanghai, China

[3] Department of Rehabilitation Sciences

The Hong Kong Polytechnic University, Hong Kong, China

[*] Corresponding author: Xiao-ming Tao; email: xiao-ming.tao@polyu.edu.hk

[#] These first authors contributed equally.

Highlights:

Bionic and morphing leg mannequin constructed based on the mean value and the principal component analysis of 225 subjects

25 structured-fiber pressure sensors embedded in the bionic and morphing leg mannequin, forming a highly sensitive network for precise measurement of pressure from 0 to 10 kPa

Morphing in circumference, reducing the required number of leg mannequins for mass production

Abstract:

Compression garments, exerting appropriate pressure on the surface of needed body zones, have a wide application in medical, athletic, body-shaping, and healthcare fields. The exerted pressure, including the pressure amplitude and the special distribution, plays a significant role on the treatment efficacy. This paper presents a novel solution for pressure evaluation of precise pressure measurement of compression garments based on a smart bionic and morphing leg mannequin with 25 structured-fibre pressure sensors and 4 temperature sensing units. These pressure sensors with a high sensitivity (up to 54.7 pm/kPa with an accuracy of ~ 0.03 kPa) in the range from 0 to 10 kPa were embedded in the leg mannequin according to the German standard (RAL-GZ 387/1) and anatomical structures of ankles. Such sensor network can provide a precise pressure-mapping rather than a mean pressure obtained from other measurement systems. The fabricated leg mannequin can morph from size 23 (Size M) to 27 (Size L) with an accuracy of 0.125 mm in circumference, reducing the required leg mannequins in routine tests of manufacturing and medical applications. Furthermore, the measured pressure exerted on the fabricated mannequin was well consistent with those exerted on the human leg, showing non-uniform pressure distribution due to the apophysis and local buckles. Therefore, the characteristics of high sensitivity to low-pressure, pressure mapping, bionic, and morphing make the leg mannequins promising to be applied for routine tests in customization of compression garments.

Keywords: Bionic leg mannequins, precise pressure measurements, morphing leg mannequins, compression stockings, structured-fiber sensor arrays

1. Introduction

Compression garments like compression stockings have been widely researched and utilized in the fields of sports, healthcare, and medical applications [1-4]. Such devices can exert an appropriate pressure distribution on the needed zones, which helps increase circulation and prevent the formation of blood clots in the lower legs, and aids in the treatment of ulcers of the lower legs. The exerted pressure is one of the most important properties in efficacy, comfort, and security. Excessive pressure, that is, pressure of about 4.3 kPa and above that induced capillary closure, will make people feel discomfort, have numbness of the affected body part, or even suffer from series health issues [5, 6], and on the contrary, insufficient pressure will reduce the efficacy of treatments. Moreover, compression stockings are designed to have pressure gradient, that is, pressure gradually reduces from ankle toward knee and thigh [7, 8]. However, inappropriate pressure frequently is exerted on human legs due to relaxation of compression stockings, and more commonly, incorrect selection in terms of sizes and shapes. For example, clinical surveys showed that a significant proportion, that is, 20 - 43% [9], of hospitalized patients wore the incorrect compression stockings, which reduces the efficacy or even causes negative effects. Furthermore, human legs have a wide variety in shapes and sizes due to difference in sex, age, races, regions, and life habits, and limited sizes of compression stockings cannot fully satisfy the requires. And thus, individual customization of the compression stockings is highly desirable.

Precise assessment of the exerted pressure on the needed zone is necessary for compression garments. Such assessment relies on the properties and the reliability of the utilized fiber/yarns, the designed textile structures, and the precise and reliable pressure-measurement systems. Direct pressure measurements on the human leg can reflect the real current-value exerted from compression stockings, but inconvenient and impractical for routine tests. Because such measurements have limitations, including needs of execution by professionals, poor

repeatability of the leg-shape, and needs of the subject to be always standby. And thus, indirect measurement has been extensively studied and obtained substantive results. For example, pressure exerted on human legs was predicted based on different strategies: (1) a combination of the local body curvature with the biaxial extension properties of elastic fabrics and Laplace's Law [10-13], (2) a hypothetical leg mannequin (2D), that is, an adjustable former, and pressure at a measuring point [14], and (3) a hypothetical leg mannequin (3D) with circular cross-sections from ankle to thigh and pressure at measuring points[15]. These measurement systems are convenient and feasible for routine tests in manufactures and researches. However, the exerted pressure is predicted based on a uniform pressure-distribution, which deviates from practical states, that is, nonuniform pressure distribution induced by the irregular curvature, bony prominence and uneven mechanical properties of the leg. Accordingly, a bionic leg manikin is highly necessary for the pressure evaluation of compression garments.

Human legs widely vary in shapes and sizes, resulting in that many leg mannequins are required for the evaluation of compression stockings, such as, dozens of leg manikins are presented in the Germany Standard of RAL-GZ387/1[15]. To reduce the required leg mannequins, morphing leg mannequin [16, 17] and finite element methods [18-21] have been developed. Finite element methods first construct models of human legs and the compression garment to mimic their mechanical properties, the shape and the size, and then simulate the amplitude and the distribution of the exerted pressure on the human leg [18-21]. But such results still differ with the practical state in terms of magnitude and localized distribution, because these simulation cannot recreate the real wearing states completely, including the real mechanical properties of the fibers, which composites the compression garments, the real textiles structures after deformation and the movement of fibers induced by interactions between the human body and the compression garments. A novel measurement system of MST Professional 2 SAG [16] and a laboratory-fabricated leg mannequin [17] can represent different human legs by adjusting

the circumference, which highly reduce the required number of leg mannequins. However, the exerted pressure significantly relies on the localized mechanical properties and shapes. Based on these hard devices, the pressure assessment of compression garments may be over-predicted. Nevertheless, studies that focus on soft leg mannequins have been scarce, mainly due to complexity of construction of soft leg mannequin and inconformity of the uniform pressure assumption in measurements. Moreover, the current leg mannequins are probably not enough to satisfy the increasing requirement of the precise pressure assessment for individual customization of compression garments due to their rough classification.

This paper presents a bionic and morphing leg mannequin with highly sensitive pressure sensor networks, which can provide precise pressure measurement for routine tests and individual customization of compression garments.

2. Structural design and materials

2.1 Data extraction and analysis

To demo the geometric construction of the bionic leg mannequin, 225 subjects, including 142 females and 83 males, participated in 3D body scanning. All subjects reside in Hong Kong, 92 % of them were within 40 and 60 years-old, and people of such ages were reported as the major sufferer of chronic venous insufficiency (CVI) [22]. Most of subjects claimed suffering from knee paint and were preliminarily diagnosed as with various veins on one or both legs. And thus, they are the target users of compression garments like medical compression stockings. The research based on these subjects can provide important information for the design of leg mannequins as well as the optimal design of medical compression stockings.

Full-scale 3D body-scanning was performed on NX-16 automatic full-body scanner ($[TC]^2$, NC, USA) with the resolution of 5 degrees in the circumferential direction and 1 mm in the

height direction. Subjects wore underwear only and stood still in scanning booth in a proposed pose, with both hands holding the fixed handles while the feet kept within the marked area, which ensures the profile of both legs was fully captured. Though a slight difference exists between both legs, the left and right compression stocking of each pair are assumed to be same in practice. Thus, left legs were chosen for analysis since most of subjects were right-handed, whose left legs normally responded for more standing and more likely suffered from CVI. The extraction from 3D body-scanning data included three major steps. Step 1: Scanning data of the left leg was identified based on autonomy of human leg, where the crotch is identified as the upper limit and the ankle is identified as the lower limit (**Figure 1a and 1b**). Step 2: Since the initial angle between the leg and the floor slightly deviates from 90^{o} for capturing the data of thighs, slight rotation was also performed by making the straight line between the cross-section centres of the ankle and the thigh-root become vertical, as shown in **Figure 1c**. Step 3: For data normalization, a new dataset was sampled by interpolation, having 72 points for each cross-section and 200 equidistant cross-sections from ankle to thigh, as shown in **Figure 1d** and the inset figure.

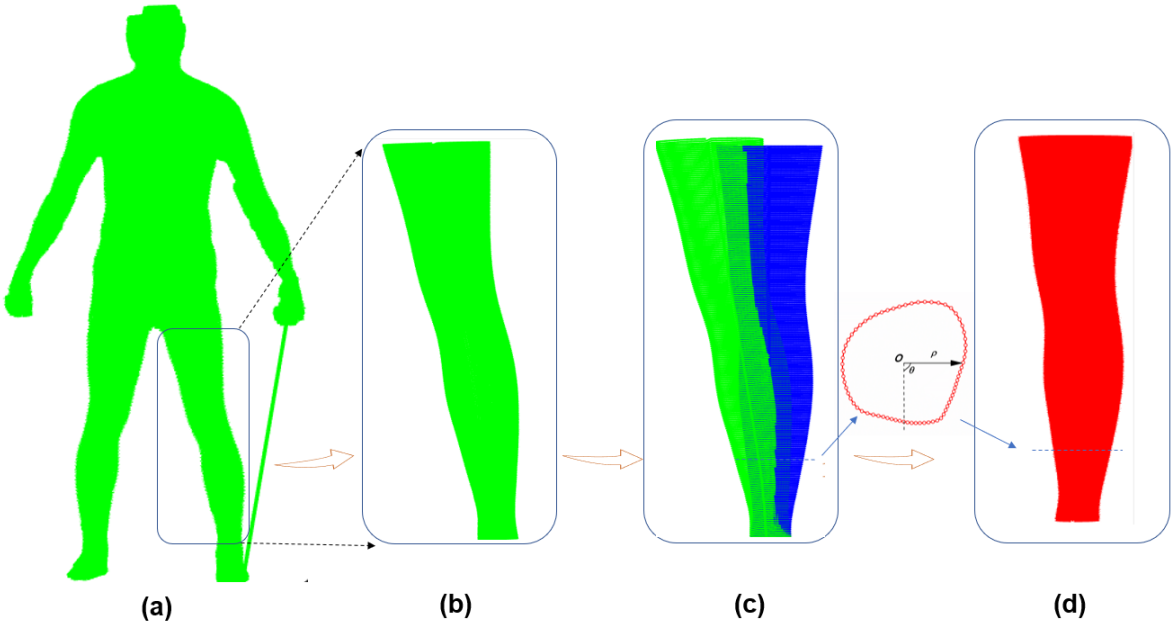

Figure 1. (a) Illustrated data of 3D body-scanning, (b) Identification and extraction of the leg according to anatomy of human legs, (c) Rotation of the extracted leg to make it upright so that each section is parallel to the horizontal plane, and (d) Resampling for date nominalization.

Compression garments exerted the circumference stress, that is lateral pressure, on the surface of needed body zones by tension of elastic yarns/fabric. And thus, circumference is one significant parameter in the pressure measurement and the design of compression stockings. The circumference, C, of the digital leg mannequin can be estimated through the point-to-point integration along the boundary.

$$C = \oint dl = |P_1 - P_N| + \sum_{i=1}^{N-1} |P_i - P_{i+1}| \quad (1)$$

where N is the max sequential number of points, P_i.

3D principal component analysis (PCA) was performed to determine the principal components of the profiles of legs. The principle components (PCs), representing the main characteristics of the leg profiles, were sorted in an order of their importance. The percentiles and the eigen values of the first 10 PCs are listed in **Table 1**, showing that the first 3 PCs can explain ~ 92.62 % profile variations in total. These PCs physically reflect the variation of circumference, the bulging level of the knee, and whether the thigh and calf are more consistently symmetrical or curvy on the leg profiles, respectively. Among these PCs, the first PC, reflecting the variation of circumference, explains ~ 77.00 % profile variations.

Table 1. The eigen values and percentage of variance of the first 10 PCs

Principal components	Eigen value	Variance
PC1	1.0911*10^5	77.00%
PC2	1.4130*10^4	9.97%
PC3	8.0006*10^3	5.65%
PC4	3.7259*10^3	2.63%
PC5	2.4669*10^3	1.74%
PC6	1.6684*10^3	1.18%

PC7	1.1327*10^3	0.08%
PC8	612.9151	0.43%
PC9	302.5480	0.21%
PC10	169.3158	0.12%

The height of legs from ankle to tight was normalized: the height of the ankle is zero, and the end of the tight is one. After normalization, the circumferential profiles of all subjects are illustrated in **Figure 2a**, showing a non-linear relationship between the height and the mean circumference. The circumference variation can be vast from one subject to other subjects. Thus, leg mannequins with different size are necessary in practice. Twenty-six sizes of the leg mannequin with the same height are listed in the German standard for medical compression hosiery [15]. As illustrated in **Figure 2b**, the circumference variance of the leg mannequin from one size to other size is a polyline, where the measuring points is consistent with the German standard [15] and also similar to the points shown in **Figure 4b**. Accordingly, the variation of circumference, $\delta(z)$, along the height can be given by

$$\delta(z) = \begin{cases} a_1 \cdot z + b_1, & 0 \le z \le h_E \\ a_2 \cdot z + b_2, & h_E \le z \le h_F \\ a_3 \cdot z + b_3, & h_F \le z \end{cases} \quad (2)$$

where z is the standardized height of the leg, a_1, b_1, a_2, b_2, a_3 and b_3 are parameters, which can be identified according to PC1. h_E and h_F are the critical height of the polyline, .

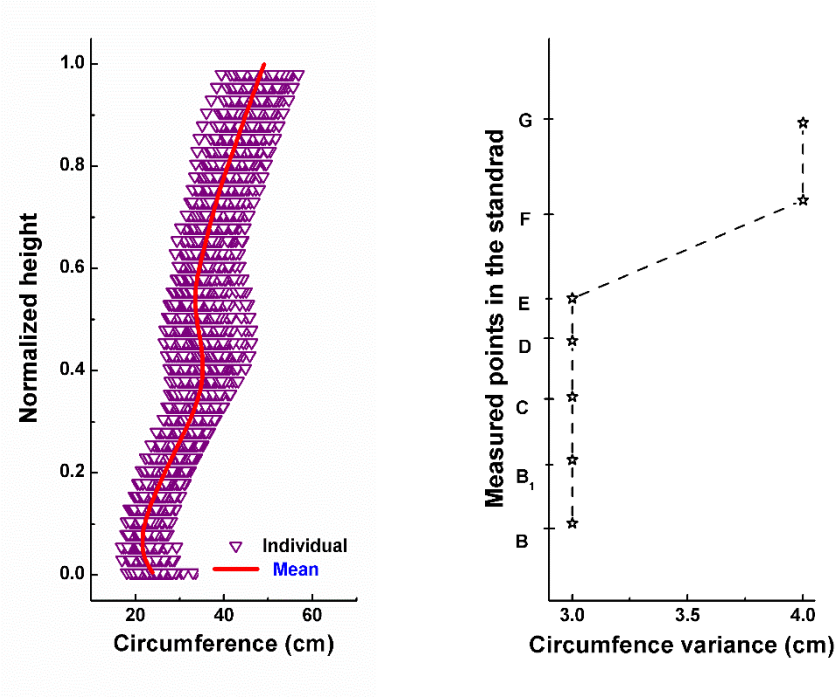

(a) (b)

Figure 2. (a) Circumferential profiles of the scanned subjects, and (b) Illustrated circumference variance between size 24 (corresponding to M size) and 27 (corresponding to L size) in the German standard for medical compression hosiery[15].

2.2 Design of 3D bionic and morphing leg mannequin

A leg mannequin can morph form one size to other sizes, that is, one leg mannequin can represent a series of human legs or leg mannequins, which is highly desirable in the routine tests of manufactories and medicinal applications. Based on the above analysis, the variance of circumference along the height is the most important parameters, which can explain ~ 77% of the profile variations shown in **Table 1**. And the circumference variance can be given in a polyline formula as equation (2). Thus, the circumferential profile at the zones of calf (from B to E) and tight (from F to G) can be achieved through varying the circumferential profile linearly.

The scanned point of each cross-section, shown in the inset of **Figure 1**, can be described in the cylindrical coordinate. If the angle and the normalized height of the measured point are given, the average radial distance, $\bar{\rho}$, of each point among subjects can be given by

$$\bar{\rho} = \frac{1}{M}\sum_{j=1}^{M} \rho_j \tag{3}$$

where M is the total number of the scanned subjects. And then, the mean leg mannequin can be obtained from $\bar{\rho}$.

To illustrate a morphing leg mannequin, the leg mannequin was separated into halves, i.e., anterior half leg and posterior half leg. The posterior half leg can move backward and recover to the initial state. The interface between the halves was set to where the line segment reaches its maximum, as shown in **Figure 3a** and **3b**. In this way, the circumferential profile, $C(z)$, can be controlled through adjusting the distance between halves. From equation (1), the circumference after morphing can be estimated by

$$C(z) = C_0(z) + 2\delta(z) \tag{4}$$

where $\delta(z)$ is the gap distance and $C_0(z)$ is the initial circumference before morphing. Accordingly, a bionic and morphing leg mannequin was designed and shown in **Figure 3c**. The leg mannequin comprises a fixed part marked in gay and a moving part marked in blue. The moving part can laterally move through three motor systems.

As shown in **Figure 4a**, four sensor arrays were designed and marked in red: two arrays in the front side marked by “1” and “2”, one array in the right side marked by “3”, and one array in the left side marked by “4”. And the sensor array marked in “1” was set on the tibia. The compression stockings probably exert non-uniform pressure on the surface near ankles due to the local bulges and buckles. And thus, twenty-one measuring points from B to G were designed according to the German standard of Medical Compression Hosiery [15], three

measuring points of A_0 were added near ankle, and one measuring point of A_1 was added on the instep, as shown in **Figure 4b**. Moreover, since the structured-fiber pressure sensors are also sensitive to the change of temperature, one temperature sensing unit, that is, bare Bragg gratings fabricated in a casing pipe and then embedded in the silicone matrix, was set up at the end of each sensor array for monitoring temperature changes.

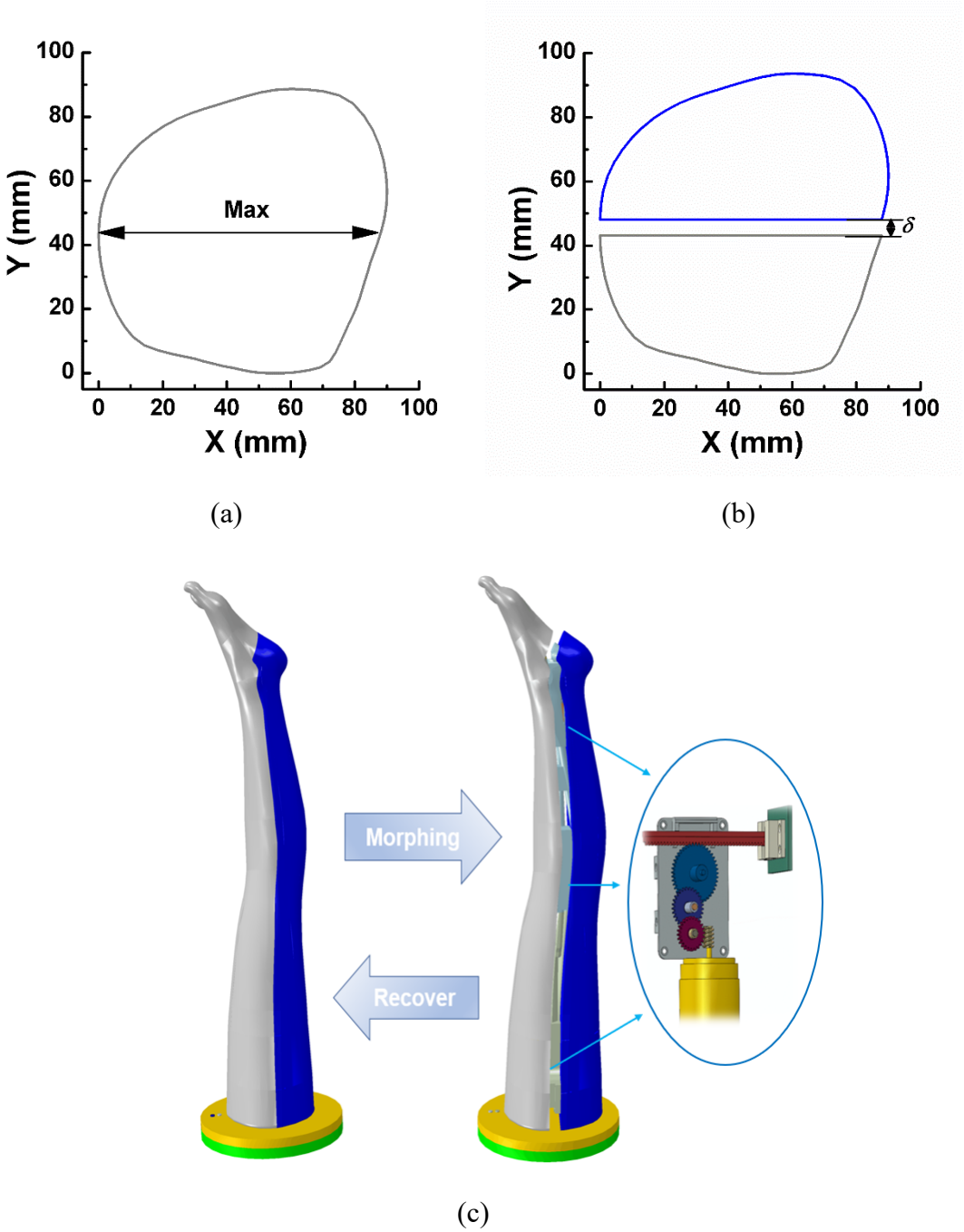

Figure 3. Schematic of determining the location of interface between halves of the cross-section of leg at the normalized height of 0.25 : (a) before morphing and (b) after morphing; and (c) Schematic of the bionic and morphing leg mannequin.

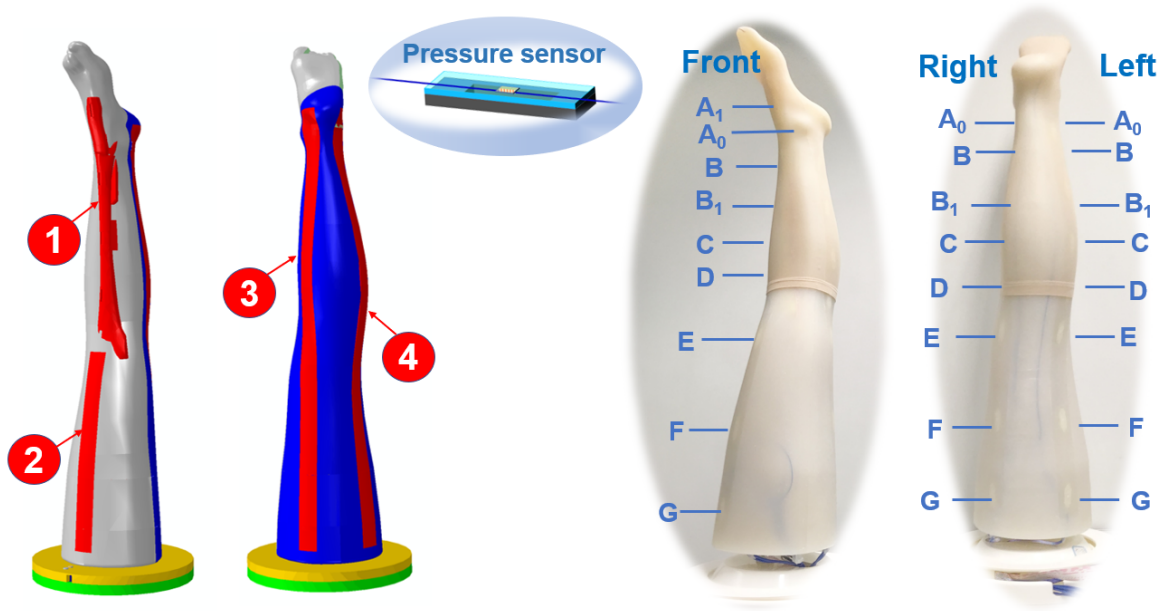

(a) (b)

Figure 4. (a) Four sensor arrays of the leg mannequin, and (b)The fabricated leg mannequin, wearing a short silk stocking, and schematic of pressure measuring points, where the inset is the schematic of structured-fiber pressure sensors.

2.3 Materials and fabrication

The leg mannequin consists of tissues made of silicone, bones made of Acrylonitrile Butadiene Styrene (ABS), motors systems and novel structured-fiber pressure sensor arrays. Silicone (type of 903, China) was adopted for its excellent elasticity, appropriate elastic modulus of ~ 1.3 MPa similar to that of a typical soft tissue (~ 1 MPa) [23], and facile fabrication. Moreover, such silicone has an approximately linear relationship between stress and strain and low hysteresis within the range below 25 kPa [24]. The material of ABS has higher elastic modulus, three orders higher than that of silicone, and is easy of processing in 3D numerical controlled machine tools. The exerted pressure can be measured via mechanical [25], electrical [26-31]and optical signals [24, 32, 33]. Related to electrical sensors and mechanical sensors, optical sensors have specific merits of high sensitivity to small deformation, robustness, good immunity to electromagnetic interference, no electricity at measuring points, and ease of

integration. The exerted pressure on the fabricated leg mannequin is normally small, such as from 3.1 to 4.3 kPa for class II compression stockings [15], which induce small deformation on the leg mannequin. Thus, optical fiber sensors were selected for the application. Similarly to those in [24], structured-fiber pressure sensors comprise an optical fiber (SMF-28®ultra-optical fibre, Corning Inc., USA) with Bragg gratings, a rigid base with a rectangular groove, a spacer and a thin film, as shown in the inset of **Figure 4**. Such structure effectively converts the applied pressure into axial tension of Bragg gratings.

There are seven steps included during the fabrication. Step 1: Similarly to the steps in [24], the structured-fiber pressure sensor arrays were fabricated firstly. The leg mannequin is bionic and has structures of bones. As shown in **Figure 5**, the tibia is very close to the skin, and thus, the pressure sensing units were fabricated on the tibia directly. Other three sensor arrays were in form of belts, as shown in **Figure 4a**. Step 2: According to the schematic shown in **Figure 3b**, three step motor systems were developed by using a step motor, transfer structure for movement of the moving part and safety. Step 3: Models for injection of silicone, bones, and pillars for locations were developed based on the above designs, including the split leg mannequin, sensor arrays, and motor systems. Step 4: Silicone mixture (Type of 903, A: B=100:1 in weight ratio) after vacuum pumping was injected into the models, fabricating the fixed part and the moving part of a leg mannequin, respectively. Step 5: The whole set was placed on a horizonal table and held for over 8 hours at room temperature, until the curing process was completed. Step 6: The fixed part and the moving part of the leg mannequin were taken out from the moulds. Step 7: The motor systems were added on the leg mannequin. The fabricated leg mannequin is shown in **Figure 4b**.

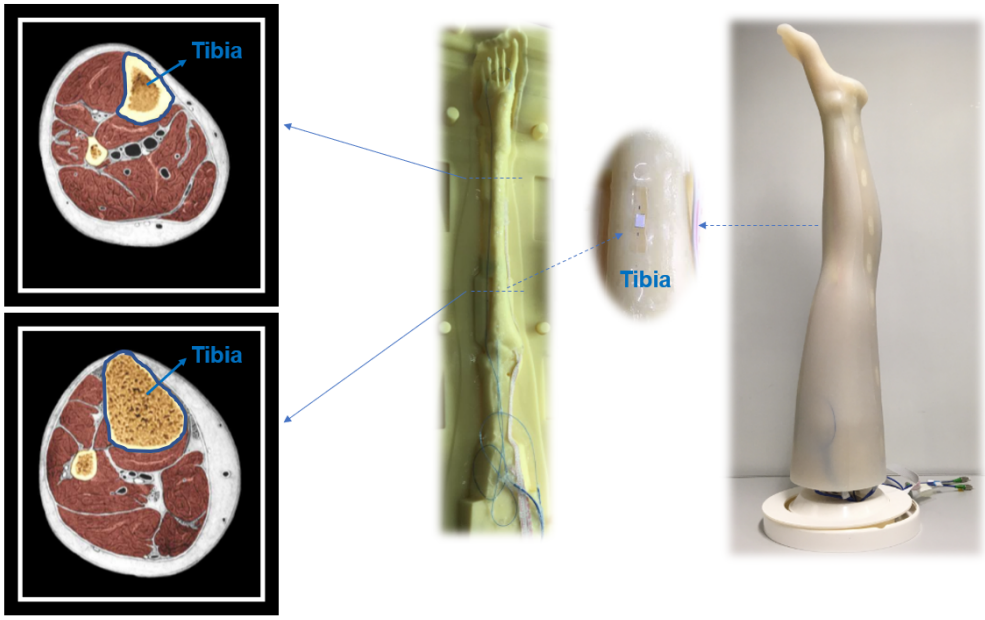

Figure 5. Schematic of cross-section of shank like the reference [34], tibia made of ABS with pressure sensing units and the fabricated leg mannequin

3. Performance of 3D bionic and morphing leg mannequin

3.1 Pressure calibration system

As shown in **Figure 4b**, the pressure sensors were embedded on a curved surface of the leg mannequin. Normal calibration methods, such as quasi-static compression performed on the material machines, become inapplicable for the leg mannequin due to the large size and the irregular surface. Therefore, a novel calibration system was utilized to provide uniform pressure. The calibration system comprises an air tank, a compressed-air source, an air pressure governor, a digital pressure gauge, a digital temperature meter, an optical interrogator and a computer, as shown in **Figure 6a**. The air tank is large and has enough space for placing the fabricated leg mannequin inside, where the diameter and the height are 50 cm and 100 cm, respectively. It needs about 30 seconds to reach balance at each increment of 0.5 kPa, and it needs over 60 seconds at each reduction of 0.5 kPa. The digital temperature meter with a

precision of 0.1℃ monitors the temperature change inside the chamber, ensuring that the temperature is constant during the measurement. The digital pressure gauge (MIK-Y190-1, China) has an accuracy of ~ 0.05 kPa (0.2%FS) and the measured range from 0 to 25 kPa. The optical interrogator (six 155-Micron Optic, Micro Optics Inc., Atlanta, GA, USA) utilized in tests has a high sampling rate of 1000 Hz, a wavelength accuracy of 1 pm and a resolution of up to 0.01 pm, and thus, it can thus provide a reliable and accurate measurement for dynamic tests.

The wavelength of FBGs at the pressure of zero, that is, the first measured point of the loading cycle, was defined to be the initial state, which is utilized for the calculation of the wavelength shift, $\Delta\lambda$. Similar to the performance of the fabricated structed-fiber pressure sensors in [24], when the temperature is constant, the relationships between the wavelength shift of FBGs and the applied pressure are linear, illustrated in **Figure 6b ~ d**. The wavelength shifts of the temperature sensing unit, shown in **Figure 6e**, are close to zero, indicating that the temperature sensing unit is insensitive to the applied pressure.

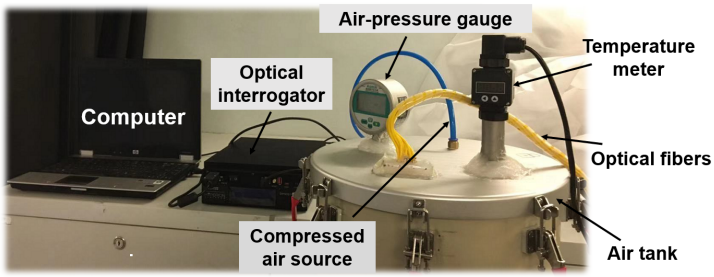

(a)

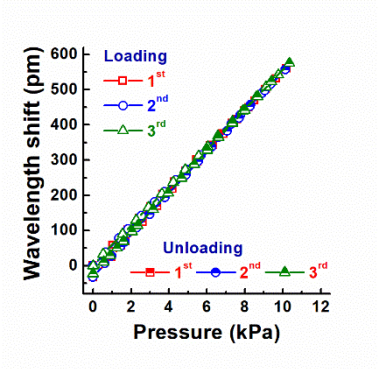

(b)

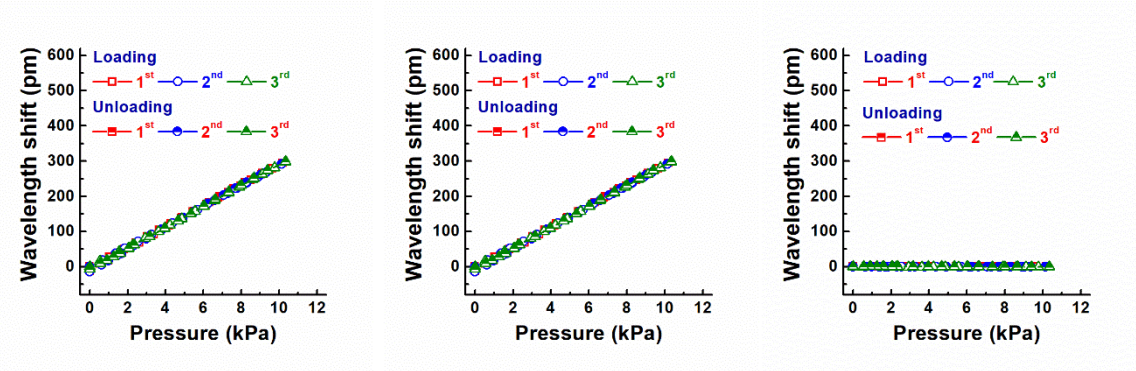

Figure 6. (a) Schematic of the calibration system, Illustration of the calibration results at the measuring point of B: (b) Front, (c) Right, (d) Left, and (e) The temperature sensing unit at the array 1, where the room temperature was 21.1 ± 0.1 ℃.

3.2 Pressure sensitivity

When the temperature is constant, like the leg mannequin is utilized in a standard lab with constant temperature, the wavelength shift linearly changes with increasing or decreasing of the applied pressure, as shown in **Figure 6**. The corresponding sensitivities, that is, the slope of the curve, are listed in **Table 2**. Four sensors of A_0, B_1, C and D in the front of the leg mannequin show weak sensitivity to the applied pressure. Among these sensors, A0 and B1 even show weak fitting coefficient. Because a thick silicone layer (over 3 mm) covered on the fabricated sensors, where optical pressure sensors may be damaged, was induced by the inaccurate fixture of the tibia model during the manufacture. Excluding these four sensors, the sensitivity of the fabricated sensors ranges from 12.7 to 54.7 pm/kPa, showing a high sensitivity. And then, the exerted pressure, p, can be estimated easily form the wavelength shift of FBGs.

$$p = \Delta\lambda / C_p \tag{5}$$

where C_p is the sensitivity to the applied pressure.

Table 2. Pressure sensitivity of sensors embedded in the leg mannequin

Measured Points	Sensitivity, C_p, (pm/kPa) [Fitting coefficient]		
	Front	Right	Left
A_1	26.5 [0.898]	-	-

A_0	-1.7 [0.789]	41.3 [0.996]	12.7 [0.973]
B	54.7 [0.995]	28.8 [0.998]	45.6 [0.987]
B_1	0.5 [0.407]	32.0 [0.987]	34.7 [0.981]
C	-	32.7 [0.993]	14.8 [0.977]
D	0.3 [0.980]	33.6 [0.994]	30.6 [0.997]
E	27.0 [0.996]	42.9 [0.998]	36.5 [0.927]
F	25.4 [0.997]	25.6 [0.959]	37.3 [0.983]
G	34.8 [0.994]	41.8 [0.997]	44.0 [0.983]

3.3 Temperature effect

Fiber Bragg grating sensors are sensitive to the changes of strain and temperature [35, 36]. Though the fabricated leg mannequin is suggested to be utilized in a standard lab, the temperature effect was also investigated by using an environment chamber of VOTSCH C7-600. The measured temperature ranges from ~ 4 to 50 ℃ with an interval of 5℃, according to the local temperature change of Hong Kong. The utilized chamber has a series of fine adjustments of temperature during the testing, aiming to hold the given temperature. Such chamber has the accuracy of temperature is about 1℃. Though each temperature increment was holding for 120 minutes, the fabricated leg mannequin cannot reach temperature balance in a short time after the fine adjustment of temperature. Because the leg mannequin has a large volume and the heat transfer from air to the mannequin is weak. Therefore, the recorded temperature of the thermometer in the air may be slightly different from the actual temperature of the embedded sensors of the fabricated leg mannequin, inducing that some wavelengths of the fabricated sensors at the same recorded temperature also show a slight difference, as shown in **Figure 7**.

As shown in **Figure 6e,** the wavelength of the illustrated temperature sensing unit is insensitive to the applied pressure. The calibration result in the environment chamber shows that such

fabricated sensor has a linear relationship between the temperature change and the wavelength shift of FBGs, and its sensitivity to the temperature change is about 9.7 pm/℃ (close to 10 pm/℃ of bare FBGs [36]), as shown in **Figure 7a**. The calibration result of the structured-fiber pressure sensor shows a higher sensitivity to the temperature changes, having a nonlinear relationship between the wavelength and the temperature as illustrated in **Figure 7b**. Because such structured-fiber pressure sensor is made of materials with different thermal expansion, such as silicone (~ 300×10^{-6}/℃), ABS (~ 72×10^{-6}/℃) and silica (~ 0.55×10^{-6}/℃) [24]. If the temperature of the environment changes, those components will be reached new stress balance, as well as changing the wavelength of FBGs.

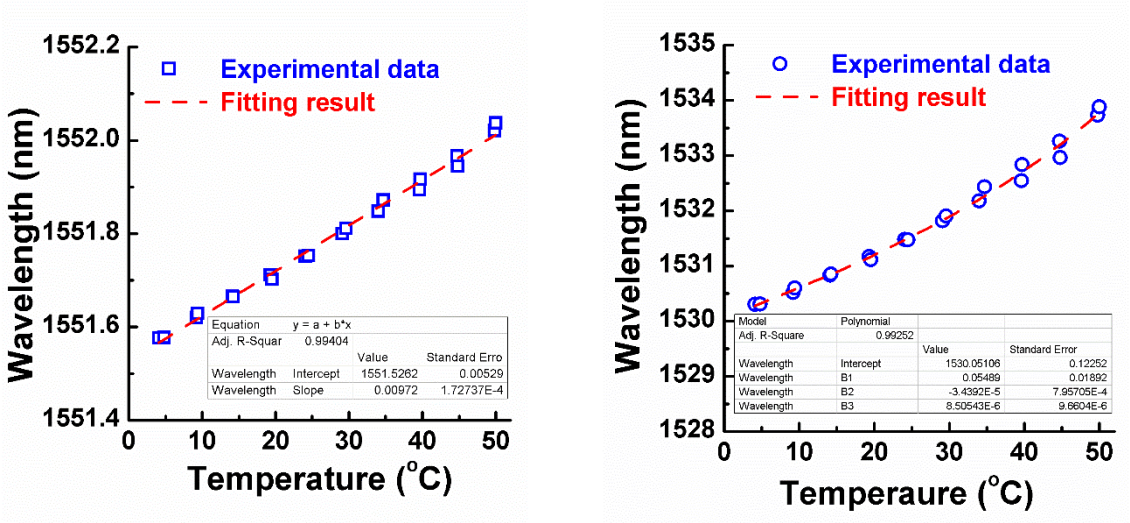

(a) (b)

Figure 7. Illustrated calibration results of sensing units embedded in the leg mannequin: (a) Temperature sensing units and (b) Structured-fiber pressure sensors.

3.4 Morphing of 3D bionic leg mannequin

As shown in **Figure 3c**, three step motor systems were utilized to control the morphing of the leg mannequin. The circumference adjustment of each motor system is different because the utilized tracks have different length, which is limited by the diameter of the cross-section of

the fabricated leg mannequin. Thus, the motor system near ankle has min range of the circumference adjustment from zero to over 4 cm. And other two motor systems have wider adjustment ranges, which can be up to 6 cm and 10 cm, respectively. According to the German standard for medical compression hosiery[15] shown in **Table 3**, the fabricated leg mannequin can morph from size 23 to 27 marked in green, that is, from size M to L, meaning that one fabricated leg mannequin can utilized in over 5 sizes. Thus, the required leg mannequin can be reduced. Moreover, the morphing range of the leg mannequin can be changed if needed.

Though the leg mannequins have a series of sizes, the actual size of human legs have huge amounts of size due to difference in races, sex, age, regions, working and living habits. Thus, more precise classification of leg mannequins are highly desirable for customized compression garments. Because a leg mannequin is closer to the real human leg, it can more accurately assess the actual pressure from the compression stockings. In the fabricated leg mannequin, three step motor systems can be controlled individually to adjust the circumference with a high precision of 16 rotations/mm. It means that the circumference can be adjusted at a high accuracy of ~ 0.125 mm within the range from size 23 to 27 cm. Therefore, such morphing leg mannequin can be well satisfied the requirement of precise size and promise to be a good candidate for routine tests in customization of compression garments.

Table 3. Leg circumferences and size of leg mannequins in the German standard for medical compression hosiery [15]

Leg circumference and size																									
Circu-mference code	Slender supplement					Size*													Slender supplement						
						18	19	20	21	22	23	24	25	26	27	28	29	30								
									S			**M**			**L**		**XL**								
Circumference in cm																									
cG	43	45	46	48	49	51	52	54	55	57	**58**	**60**	**61**	**63**	**64**	66	67	69	70	72	73	74	76	77	79	80
cF	35	37	38	40	41	43	44	46	47	49	**50**	**52**	**53**	**55**	**56**	58	59	60	61	62	63	65	66	68	69	71
cE	30	31	32	33	34	35	36	37	38	39	**40**	**41**	**42**	**43**	**44**	45	46	47	48	49	50	51	52	53	54	–
cD	25	26	27	28	29	30	31	32	33	34	**35**	**36**	**37**	**38**	**39**	40	41	42	43	44	45	46	47	49	–	–
cC	26	27	28	29	30	31	32	33	34	35	**36**	**37**	**38**	**39**	**40**	41	42	43	44	45	46	47	48	–	–	–
cB1	19	20	21	22	23	24	25	26	27	28	**29**	**30**	**31**	**32**	**33**	34	35	36	37	38	39	40	–	–	–	–
cB	–	–	15	16	17	18	19	20	21	22	**23**	**24**	**25**	**26**	**27**	28	29	30	31	32	33	–	–	–	–	–
cA	–	–	15	16	17	18	19	20	21	22	**23**	**24**	**25**	**26**	**27**	28	29	30	31	32	33	–	–	–	–	–
cY	–	–	–	–	–	–	28	29	30	31	**32**	**33**	**34**	**35**	**36**	37	38	–	–	–	–	–	–	–	–	–
*) correspond to circumferences cB																										

3.5 Discussion

The fabricated leg mannequin shows high sensitivity to the applied pressure and has multiple sensing arrays to measure the applied pressure gradient, as shown in **Figure 6** and **Figure 4**. , respectively. These calibration results were performed on a uniform pressure provided by the compressed air. While the exerted pressure on the human leg is performed by tension of elastic fabric, forming a direct compression on the surface. Thus, the measured pressure from different loading methods was investigated. As shown in **Figure 8**, an air pocket was utilized to mimic the pressure exerted from compression garments. The wavelength shifts of FBGs induced by an air pocket are well consistent with those induced by the compression air in the tank, which indicated that within the investigated pressure range, the calibration method based on compressed air is reasonable.

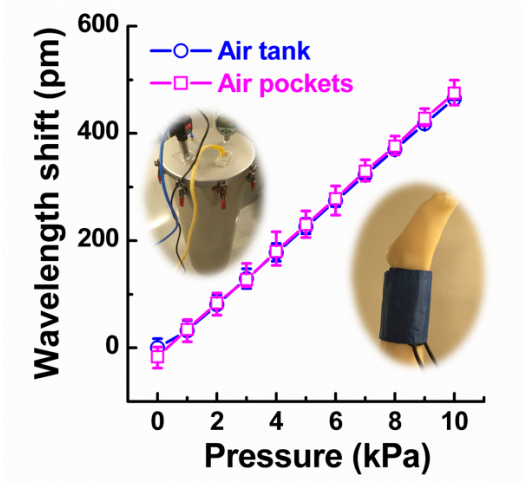

Figure 8. Comparison of the wavelength shift at the measuring point of B induced by different loading methods, including pressure provided by the compressed air in the air tank and pressure provided by an air pocket, where the room temperature was 21.1 ± 0.1 ℃ and three cycles of loading and unloading were performed.

The soft polymer of silicone was utilized in the leg mannequin and the structured-fiber pressure sensors. Such silicone is a kind of viscoelastic materials, and it needs enough time to recover

after deformation. As shown in **Figure 6b - d**, the wavelength shift of FBGs at the zero-pressure of the unloading process is slightly below zero, showing a reasonable hysteresis. Besides hysteresis, nonlinearity and repeatability also affect the accuracy of the fabricated sensors. Thus, the calibration data of three loading-unloading cycles were utilized to estimate the accuracy of the fabricated pressure sensors. And the accuracy can be given by

$$\text{Accuracy} = \pm max(\left|p_i - p_{a,i}\right|), \text{ for } i=1, 2, ..., n \quad (6)$$

where p_i is the estimated pressure at the i^{th} measurement from equation (5), $p_{a,i}$ is the actual pressure of the i^{th} measurement, and n is the total number of the measurements. The accuracy of the fabricated sensors ranges from 0.03 to 0.67 kPa, as listed in **Table 4**.

Table 4. Accuracy of sensors embedded in the fabricated leg mannequin

Measured Points	Accuracy (kPa)		
	Front	Right	Left
A_1	± 0.63	-	-
A_0	-	± 0.12	± 0.33
B	± 0.03	± 0.06	± 0.05
B_1	-	± 0.07	± 0.10
C	-	± 0.15	± 0.14
D	-	± 0.18	± 0.09
E	± 0.14	± 0.04	± 0.67
F	± 0.10	± 0.67	± 0.08
G	± 0.13	± 0.04	± 0.05

Though the fabricated leg mannequin is suggested to utilize in a standard lab with constant temperature, the environment temperature may have a slight difference among different labs. The fabricated leg mannequin was calibrated under different temperature from 19.1 to 24.1℃. As shown in **Figure 9a**, a linear relationship between the wavelength and the applied pressure is obtained under different temperature, showing an extremely similar slope. And the

corresponding wavelength shifts under different temperature are closely same, as shown in **Figure 9b**. These results indicate that their sensitivities don't need a specific correction within the investigated temperature range.

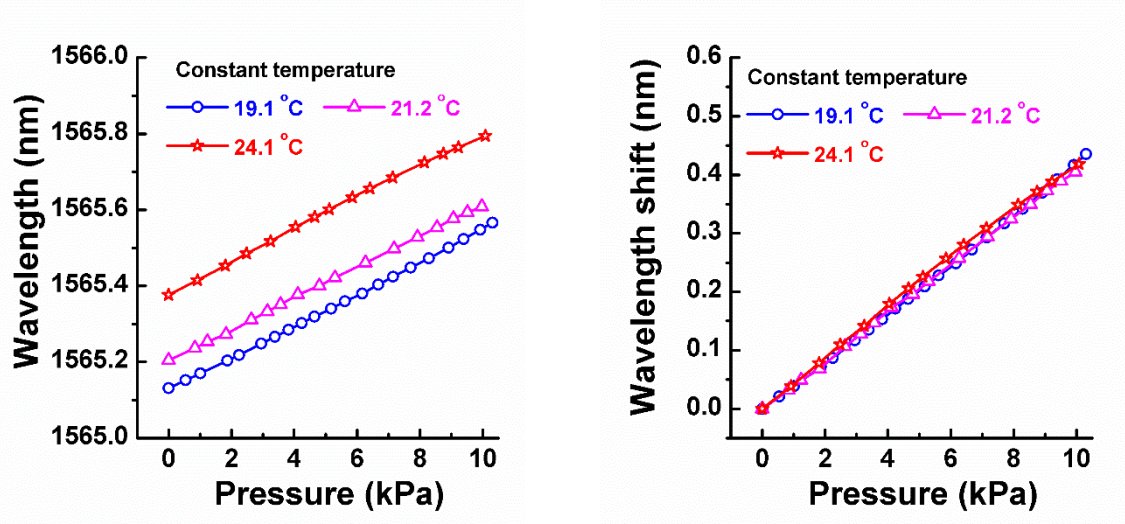

(a) (b)

Figure 9. Effect of the temperature and the applied pressure on the wavelength of the illustrated pressure sensor: (a) Wavelength versus pressure and (b) Corresponding wavelength shift versus pressure, where the temperature of each curve is constant.

If the fabricated leg mannequin is utilized in an open environment, where the applied pressure and the temperature on the leg mannequin are both changed during tests. The measured result should be corrected based on decoupling of the temperature and the pressure of the fabricated pressure sensor. Though the leg mannequin is not suggested in such environment, an approximate model based on linear decoupling was given by

$$p = \frac{\lambda - \lambda_0 - [\lambda_T(T) - \lambda_T(T_0)]}{C_p} \quad (7)$$

where λ is the wavelength of the fabricated sensor, and λ_0 represents the wavelength at the initial state of the temperature of T_0 and the pressure of zero. $\lambda_T(T)$ and $\lambda_T(T_0)$ are the wavelength of the fabricated pressure sensor at the conditions that the pressure of zero and the

temperature of T and T_0, respectively, which can be calculated through the fitting result of the calibration tests like **Figure 7b**. T and T_0 be estimated by the fitting result of the temperature sensing unit shown in **Figure 7a**.

4. Applications

As shown in **Figure 6**, the fabricated leg mannequin shows high sensitivity to low-pressure of below 10 kPa, which can be a good candidate for pressure measurement of compression garments. To illustrated this, a graphical user interface for the fabricated leg mannequin system was developed based on the software of Micro Optics ENLIGHT, as shown in **Figure 10**. Before measuring the pressure exerted from a compression stocking, the initial wavelength of FBGs should be recorded firstly. And then the real-time pressure exerted on the leg mannequin will be shown in the graphical user interface. The sampling rate of the wavelength is up to 1000 Hz and the accuracy is about 1 pm, and thus, the recorded pressure was slightly different from zero, having a reasonable variance below 175 Pa, where a silk stocking wore on the leg mannequin for reducing the friction between the compression stocking and the fabricated leg mannequin.

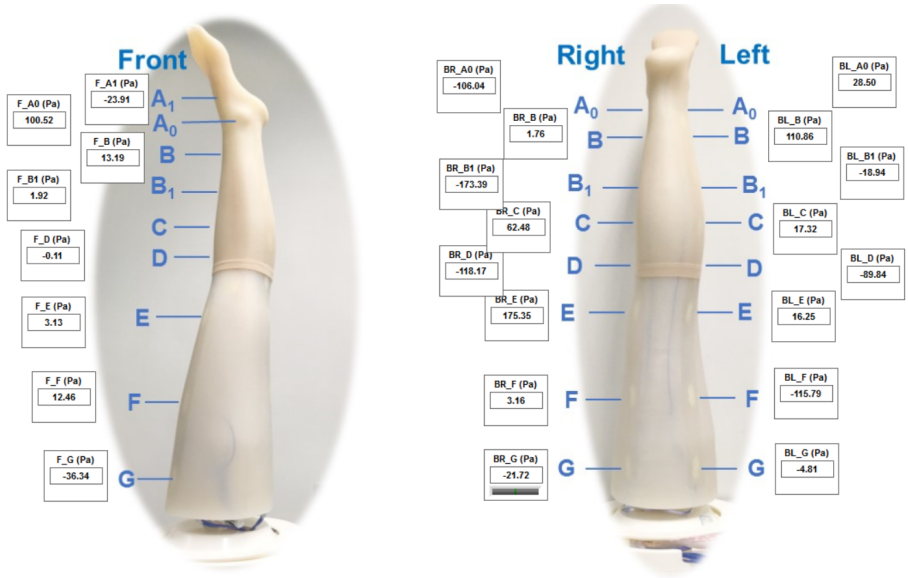

Figure 10. An illustration of the graphical user interface (before wearing a compression stockings)

To evaluate the accuracy of the pressure measurement by using the fabricated leg mannequin, the same compression stocking was measured by different organizations, including Hohenstein Laboratories in Germany (using the Compression Measurement System Hohenstein (HOSY)), SWISSLASTIC AG ST GALLEN in Switzerland (using MST MK V), and our lab (using the fabricated leg mannequin and using Kikuhime pressure sensor device to measure the exerted pressure on human legs). The pressure examination and the measuring points are according to the German standard for medical compression hosiery [15]. The circumference at the measuring point of B of the fabricated leg mannequin was adjusted to size 24, which is consistent with the circumference of the human leg and other two measurement by using HOSY and MST. As shown in **Figure 11a,** the evaluated pressure at the measuring point of B has an excellent agreement between the measurement by using HOSY and MST. Such evaluated pressure is remarkably like the measured pressure at the front and back measuring point of the human leg but higher than the measured pressure at the side measuring point. Because the exerted pressure from compression stockings relies on the local curvature of the leg. The measurement of HOSY and MST are based on the hypothetical model with circular cross-section. If the local curvature is large enough, this hypothesis is satisfied. However, the cross-section profile of human legs is irregular. As illustrated in **Figure 11b**, the local curvature of the front and left measuring point is large and convex, showing a pressure consistent with that measured by HOSY and MST. And the local curvature of the right measuring point is slightly amphicoelous, showing a lower pressure. The fabricated leg mannequin have similar cross-section to the human leg. And the pressure measured by the fabricated leg mannequin is well consistent with that measured on the human leg in terms of amplitude and positions, showing a non-uniform pressure distribution along the direction of circumference.

As shown in **Figure 11c**, the pressure mapping shows the exerted pressure decreases from ankle to knee. the manual of compression stockings. However, the actual pressure relies on the local shapes. For example, the exerted pressure on the surface at the right side of the leg mannequin is lower than that of the front size or the left side. And the pressure at the measuring point of A_0 is smaller than that at the measuring point of B due to the local buckles. These results are also agreed with the pressure measured on the human leg. Therefore, the fabricated leg mannequin system can really reflect the exerted pressure from compression stockings and provide real-time pressure gradient for the design or optimization of compression stockings.

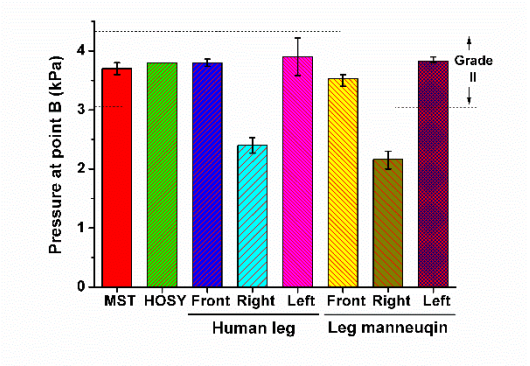

(a)

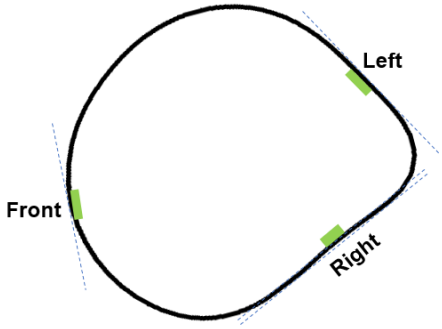

(b)

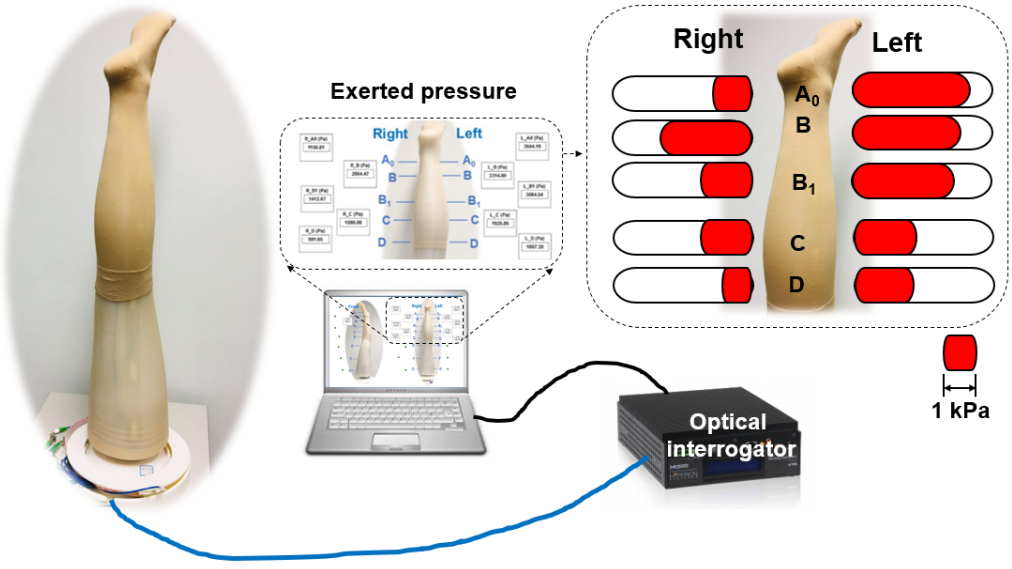

(c)

Figure 11. (a) Measured pressure at the key measuring point of B obtained from different systems, including MST, HOSY, the Kikuhime pressure sensor on human leg and the

fabricated leg mannequin, (b) Profile of the cross-section at the measuring point B of the fabricated leg mannequin, which is like that of the human leg, and (c) Pressure mapping where a commercial compression stockings (Grade II) was wearing on the fabricated leg mannequin.

5. Conclusions

Based on the PCA analysis of 3D scanning data and novel structured-fiber pressure sensors, we have designed, fabricated and tested a morphing and bionic leg mannequin system. Twenty-five pressure sensors were setup in the leg mannequin according to the common standard and anatomical structure of ankles, forming a pressure sensing network. And these sensors have high sensitivity (up to 54.7 pm/kPa with an accuracy of ~ 0.03 kPa) within the pressure range from zero to 10 kPa. The measured pressure on the fabricated mannequin was well consistent with that of direct measurement at the human leg, showing non-uniform pressure due to apophysis and local buckles. Moreover, the results of PCA analysis show that variance of circumference is the most important parameters, reflecting ~ 77% of the leg variety among the scanned subjects. Based on the 3D scanning data and PCA analysis, the fabricated leg mannequin has been fabricated and can morph from size 23 to 27 with a high accuracy of 0.125 mm in circumference, which can effectively reduce the amount of the required leg mannequins. The fabricated leg mannequin is bionic in the item of geometry and mechanical properties. High sensitivity to low-pressure, pressure mapping, bionic, morphing of the fabricated leg mannequins make it be a novel and effective tool for precise pressure assessing in routine tests of compression garments.

Acknowledgments

The authors acknowledge financial support from the Research Grants Council, Hong Kong (Project no. 525113, 15215214, 15211016, 15200917), Hong Kong Polytechnic University,

Hong Kong (Project no. 1-BBA3), and Innovation and Technology Commission, Hong Kong SAR Government (Project no. ITP/039/16TP).

References

[1] O.T. Castilho, N.R.A. Dezotti, M.B. Dalio, E.E. Joviliano, C.E. Piccinato 2018, Effect of graduated compression stockings on venous lower limb hemodynamics in healthy amateur runners, *J Vasc Surg-Venous L*, 6 83-9.
[2] Y.P. Xu, W. Wang, J. Zhao, J.H. Wang, T.T. Zhao 2019, Knowledge, attitude, and practice of healthcare professionals toward clinically applying graduated compression stockings: results of a Chinese web-based survey, *J Thromb Thrombolys*, 47 102-8.
[3] D.B. Hobson, T.Y. Chang, J.K. Aboagye, B.D. Lau, H.M. Shihab, B. Fisher, S. Young, N. Sujeta, D.L. Shaffer, V.O. Popoola, P.S. Kraus, G. Knorr, N.E. Farrow, M.B. Streiff, E.R. Haut 2017, Prevalence of graduated compression stocking-associated pressure injuries in surgical intensive care units, *J Crit Care*, 40 1-6.
[4] R. Wade, E. Sideris, F. Paton, S. Rice, S. Palmer, D. Fox, N. Woolacott, E. Spackman 2015, Graduated compression stockings for the prevention of deep-vein thrombosis in postoperative surgical patients: a systematic review and economic model with a value of information analysis, *Health Technol Asses*, 19 (98):1-220. doi: 10.3310/hta19980.
[5] S. Tanaka, T. Midorikawa, H. Tokura 2006, Effects of pressure exerted on the skin by elastic cord on the core temperature, body weight loss and salivary secretion rate at 35 C, *European journal of applied physiology*, 96 471-6.
[6] M. Denton 1972, Fit, stretch, and comfort, *Textiles, 1(1), 12-17*.
[7] R. Liu, X. Guo, T.T. Lao, T. Little 2017, A critical review on compression textiles for compression therapy: Textile-based compression interventions for chronic venous insufficiency, *Text Res J*, 87 1121-41.
[8] M. Junger, K. Sippel 2003, Compression therapy for chronic venous insufficiency. New test procedures and therapeutic options, *Hautarzt*, 54 1045-52.
[9] R. Wade, F. Paton, N. Woolacott 2017, Systematic review of patient preference and adherence to the correct use of graduated compression stockings to prevent deep vein thrombosis in surgical patients, *J Adv Nurs*, 73 336-48.
[10] L. Macintyre, R. Ferguson 2013, Pressure garment design tool to monitor exerted pressures, *Burns*, 39 1073-82.
[11] L.Macintyre, M.Baird, and P.Weedall 2004, The study of pressure deliveryfor hypertrophic scar treatment, International Journal of Clothing Science andTechnology, 16(1/2):173-183. https://doi.org/10.1108/09556220410520450.
[12] L. Macintyre, M. Baird 2006, Pressure garments for use in the treatment of hypertrophic scars - a review of the problems associated with their use, *Burns*, 32 10-5.
[13] W. Kirk Jr, S. Ibrahim 1966, Fundamental relationship of fabric extensibility to anthropometric requirements and garment performance, *Text Res J*, 36 37-47.
[14] B.S. Institution 1985, British Standard Specification for graduated compression hosiery BS 6612.
[15] D.I.f.G.u.K. E.V. 2008, Medical Compression Hosiery, Quality Assurance RAL-GZ 387/1, Beuth Verlag, Berlin.
[16] M.P. Sikka 2017, Manikins for medical textile evaluation, Manikins for Textile Evaluation, Elsevier259-77.

[17] M. Hirai, H. Partsch 2013, The Mannequin-leg: a new instrument to assess stiffness of compression materials, *Veins and Lymphatics*, 2 3.
[18] Y.L. Lin, K.F. Choi, A. Luximon, L. Yao, J.Y. Hu, Y. Li 2011, Finite element modeling of male leg and sportswear: contact pressure and clothing deformation, *Text Res J*, 81 1470-6.
[19] R.L.Y.L. Kwok, Y. Li, T.T. Lao, X.Q. Dai, X. Zhang 2007, Numerical simulation of internal stress profiles and three-dimensional deformations of lower extremity beneath medical graduated compression stocking (GCS), *Fiber Polym*, 8 302-8.
[20] R. Liu, Y.L. Kwok, Y. Li, T.T. Lao, X. Zhang, X.Q. Dai 2006, A three-dimensional biomechanical model for numerical simulation of dynamic pressure functional performances of graduated compression stocking (GCS), *Fiber Polym*, 7 389-97.
[21] X. Zhang, K.W. Yeung, Y. Li 2002, Numerical simulation of 3D dynamic garment pressure, *Text Res J*, 72 245-52.
[22] J.L. Beebe-Dimmer, J.R. Pfeifer, J.S. Engle, D. Schottenfeld 2005, The epidemiology of chronic venous insufficiency and varicose veins, *Ann Epidemiol*, 15 175-84.
[23] R. Akhtar, M.J. Sherratt, J.K. Cruickshank, B. Derby 2011, Characterizing the elastic properties of tissues, *Mater Today*, 14 96-105.
[24] B. Yang, S. Liu, X. Wang, R. Yin, Y. Xiong, X. Tao 2019, Highly Sensitive and Durable Structured Fibre Sensors for Low-Pressure Measurement in Smart Skin, *Sensors-Basel*, 19 1811.
[25] S. Rajala, J. Lekkala 2014, Plantar shear stress measurements - A review, *Clin Biomech*, 29 475-83.
[26] N.Q. Luo, W.X. Dai, C.L. Li, Z.Q. Zhou, L.Y. Lu, C.C.Y. Poon, S.C. Chen, Y.T. Zhang, N. Zhao 2016, Flexible Piezoresistive Sensor Patch Enabling Ultralow Power Cuffless Blood Pressure Measurement, *Advanced Functional Materials*, 26 1178-87.
[27] W.S. Na, J. Baek 2018, A Review of the Piezoelectric Electromechanical Impedance Based Structural Health Monitoring Technique for Engineering Structures, *Sensors-Basel*, 1818(5):13307.
[28] Y.Y. Wang, T. Hua, B. Zhu, Q. Li, W.J. Yi, X.M. Tao 2011, Novel fabric pressure sensors: design, fabrication, and characterization, *Smart Mater Struct*, 20(6):065015.
[29] F. Wang, B. Zhu, L. Shu, X.M. Tao 2014, Flexible pressure sensors for smart protective clothing against impact loading, *Smart Materials and Structures*, 23(1):015001.
[30] H. Kim, F. Torres, Y. Wu, D. Villagran, Y. Lin, T.-L.B. Tseng 2017, Integrated 3D printing and corona poling process of PVDF piezoelectric films for pressure sensor application, *Smart Materials and Structures*, 26 085027.
[31] Y. Wang, J. Zheng, G. Ren, P. Zhang, C. Xu 2011, A flexible piezoelectric force sensor based on PVDF fabrics, *Smart Materials and Structures*, 20 045009.
[32] M.G. Xu, L. Reekie, Y.T. Chow, J.P. Dakin 1993, Optical in-Fiber Grating High-Pressure Sensor, *Electron Lett*, 29 398-9.
[33] K. Bhowmik, G.D. Peng, Y. Luo, E. Ambikairajah, V. Lovric, W.R. Walsh, G. Rajan 2015, Experimental Study and Analysis of Hydrostatic Pressure Sensitivity of Polymer Fibre Bragg Gratings, *Journal of Lightwave Technology*, 33 2456-62.
[34] E. Limbert, J. Santy-Tomlinson 2017, Acute limb compartment syndrome in the lower leg following trauma: assessment in the intensive care unit, *Nursing Standard*, 31(34):61-71.
[35] A. Othonos, K. Kalli 1999, Fiber Bragg Gratings: Fundamentals and Applications in Telecommunications and Sensing (Artech House Optoelectronics Library), *Artech House, Boston, London*.
[36] M.M. Werneck, R.C. Allil, B.A. Ribeiro, F.V. de Nazaré 2013, A guide to fiber Bragg grating sensors, Current Trends in Short-and Long-period Fiber Gratings, InTech.